IN-34

380 363

DATE OVERRIDE

24p

TECHNICAL MEMORANDUM
X - 19

HEAT-TRANSFER AND PRESSURE MEASUREMENTS ON A FLAT-FACE

CYLINDER AT A MACH NUMBER RANGE OF 2.49 TO 4.44

By Paige B. Burbank and Robert L. Stallings, Jr.

Langley Research Center
Langley Field, Va.

Declassified August 22, 1962

NATIONAL AERONAUTICS AND SPACE ADMINISTRATION

WASHINGTON   August 1959

NATIONAL AERONAUTICS AND SPACE ADMINISTRATION

TECHNICAL MEMORANDUM X-19

HEAT-TRANSFER AND PRESSURE MEASUREMENTS ON A FLAT-FACE

CYLINDER AT A MACH NUMBER RANGE OF 2.49 TO 4.44*

By Paige B. Burbank and Robert L. Stallings, Jr.

SUMMARY

Heat-transfer coefficients and pressure distributions were obtained
on a 4-inch-diameter flat-face cylinder in the Langley Unitary Plan wind
tunnel. The measured stagnation heat-transfer coefficient agrees well
with 55 percent of the theoretical value predicted by the modified
Sibulkin method for a hemisphere. Pressure measurements indicated the
dimensionless velocity gradient parameter $\left(\dfrac{r}{a_t}\dfrac{du}{dx}\right)_{x=0}$ at the stagnation
point was approximately 0.3 and invariant throughout the Mach number
range from 2.49 to 4.44 and the Reynolds number range from 0.77×10^6 to
1.46×10^6. The heat-transfer coefficients on the cylindrical afterbody
could be predicted with reasonable accuracy by flat-plate theory at an
angle of attack of $0°$. At angles of attack the cylindrical afterbody
stagnation-line heat transfer could be computed from swept-cylinder
theory for large distances back of the nose when the Reynolds number is
based on the distance from the flow reattachment points.

INTRODUCTION

    The analysis of heating problems associated with reentry configura-
tions has led to the bluff-body concept. (See, for example, ref. 1.)
The principal reason being that bluff bodies have lower convective heat-
transfer rates at the stagnation region than sharp nose bodies and, from
geometrical considerations, allow more space for heat sink material
adjacent to the region of maximum heating. Flat-face bodies have thus
been considered for many applications where low drag is not necessarily
advantageous, that is, bodies reentering the atmosphere at near orbital
velocities. A free-flight test of such a configuration has been
reported in reference 2. The present wind-tunnel investigation was
conducted to determine the effect of Mach number, Reynolds number, and
angle of attack on the heat-transfer coefficients on a flat-face cylinder.

Pressure distributions were also measured on the configuration to provide information necessary for the computation of the heat-transfer coefficient by a modification of the method given in reference 3.

SYMBOLS

a	speed of sound, ft/sec
c_w	specific heat of model skin, Btu/lb ^{O}R
D	model diameter, 0.3333 ft
h	heat-transfer coefficient, Btu/sec-sq ft-^{O}R
k	thermal conductivity of air, Btu-ft/sec-^{O}R-sq ft
M	Mach number
ΔM	variation in free-stream Mach number
p	static pressure (unless otherwise noted), lb/sq ft
N_{Pr}	Prandtl number, 0.72
r	model radius, 0.1667 ft
R	Reynolds number based on model diameter, $\rho_\infty u_\infty D/\mu_\infty$
t	time, sec
T	temperaure, ^{O}R
u	velocity, ft/sec
w	specific weight of wall material, lb/sq ft
x,y	orthogonal coordinates on model face, ft
z	axial distance along cylindrical afterbody from leading edge, ft
α	angle of attack, deg
β	velocity gradient at stagnation point, $(du/dx)_{x=0}$
	ratio of specific heats, 1.4 for air

ρ density of air, slugs/cu ft

μ dynamic viscosity of air, slugs/ft-sec

Subscripts:

l local conditions

w   wall conditions

aw   adiabatic wall

t   stagnation

2   conditions behind normal shock

∞ free stream

n   time greater than zero

0   zero time

APPARATUS AND TESTS

This investigation was conducted in the high Mach number test section of the Langley Unitary Plan wind tunnel. This variable pressure, continuous-flow tunnel has an asymmetrical sliding-block nozzle that permits a continuous variation in the test section Mach number from 2.3 to 4.65 and is described in reference 4. The variation of free-stream Mach number in the region of the pressure model is presented in the following table:

M	ΔM
2.49	±0.01
3.51	±.02
4.44	±.01

The variation of Mach number in the region of the heat-transfer model is negligible for heat-transfer calculations.

Models

The heat-transfer coefficients and pressures were determined on separate models that were mounted side by side in the tunnel as shown in figure 1. The spacing of the two models was sufficiently large to eliminate shock interaction from one model to the other for a Mach number of 2.49 and angles of attack up to 15°. The heat-transfer model was spun from a 0.030-inch Inconel sheet and instrumented with iron-constantan thermocouples spot-welded to the inner surface of the model skin. The local skin thickness and thermocouple locations are shown in figure 2. The model was supported by a spruce core insulated from the model skin by a layer of balsa. The balsa was relieved in the vicinity of the thermocouples and the relief was vented to the free-stream static pressure to minimize heat flow to the support structure. The pressure model was machined from solid steel and instrumented with pressure orifices.

Instrumentation

The heat-transfer model was instrumented with 43 iron-constantan thermocouples. The location of the thermocouples as well as the test conditions for which each was recorded is shown in figure 2. Only the 21 thermocouples indicated by the solid symbols were used for most of the tests. The thermocouple output was recorded on a multichannel sequential analog to digital conversion system described in reference 5. The thermocouple voltages were sampled every 1/2 second and converted into digital form on a magnetic tape which in turn was fed into a punch machine for tabulation on cards.

All forty-three 0.050-inch inside-diameter pressure orifices on the pressure model were utilized for the complete range of test conditions. They were located in the same respective positions as the thermocouples shown in figure 2. The pressures were measured on manometer boards using a dibromoethylbenzene fluid and were photographically recorded.

The tunnel stagnation temperature used for the data reduction was the arithmetic average value measured by six stagnation temperature probes located across the tunnel settling chamber.

Data Reduction and Test Procedure

Pressure model.- All local pressures on the front faces were reduced to the nondimensional ratio $p_l/p_{t,2}$ where $p_{t,2}$ was measured by an orifice at the center of the flat face at an angle of attack of 0°. The

dimensionless velocity gradient parameter $\left(\dfrac{r}{a_t}\dfrac{du}{dx}\right)_{x=0}$ was determined

graphically from the plot of u_l/a_t against x/r, the term u_l/a_t being computed from the relation (from eq. (62) of ref. 6)

$$\frac{u_l}{a_t} = \left\{ \frac{2}{\gamma - 1}\left[1 - \left(\frac{p_l}{p_{t,2}}\right)^{\frac{\gamma-1}{\gamma}} \right] \right\}^{1/2} \tag{1}$$

The local measured pressures on the cylindrical afterbody are presented as local Mach number with the assumption that isentropic flow exists from the stagnation point on the model flat face.

Heat-transfer model.- The heat-transfer coefficients were obtained from transient temperature measurements, resulting from a stepwise increase in T_t, from the following relation which assumes constant temperature through the skin, negligible lateral heat flow, negligible heat flow to the backing material, and no losses due to radiation:

$$h = \frac{wc_w \dfrac{dT_w}{dt}}{T_{aw} - T_w} \tag{2}$$

In order to eliminate the determination of the slope of the curve for the variation of temperature with time, T_{aw}/T_t being assumed as a constant, the general heat-transfer equation was rewritten in the following form:

$$\frac{T_{aw}}{T_t} \int_0^t T_t \, dt - \int_0^t T_w \, dt = \frac{wc_w}{h} \int_{T_{w,0}}^{T_{w,n}} dT_w \tag{3}$$

then

$$h = \frac{wc_w\left(T_{w,n} - T_{w,0}\right)}{\left(\dfrac{T_{aw}}{T_t}\right)\sum_0^t T_t - \sum_0^t T_w}$$

in which the summations are evaluated according to the trapezoidal rule. A detailed discussion of this method of data reduction is described in reference 5.

Test procedure.- The procedure for a heat-transfer test was to run the tunnel with a cool stagnation temperature (approximately 140° F) and monitor a thermocouple on a self-balancing and recording potentiometer. When this thermocouple indicated the model had reached equilibrium, a scan of all thermocouples was recorded to determine T_{aw}/T_t. The stagnation temperature was given a stepwise increase and the thermocouple output was recorded every 1/2 second for 1 minute. The beginning time for integration was selected as the earliest time that the average tunnel stagnation temperature had reached an elevated temperature level.

Test variables.- The heat-transfer coefficient was determined at Reynolds numbers based on body diameter and free-stream conditions from 0.77×10^6 to 1.46×10^6 for Mach numbers 2.49 and 3.51 and for angles of attack of 0°, 7.5°, and 15°. The pressure distribution was determined throughout the angle-of-attack range for every 0.5 increment in Mach number from 2.49 to 4.44. Schlieren pictures and shadowgraphs, taken at low Reynolds number conditions for each point, are shown in figures 3 and 4 and are discussed subsequently.

RESULTS AND DISCUSSION

Pressure Test

The local pressures on the flat face are presented in dimensionless form in figure 5 for a Mach number of 2.49, a Reynolds number of 0.90×10^6, and angles of attack up to 15°. There was no apparent alteration of the pressure curves for a Mach number range from 2.49 to 4.44 at a constant Reynolds number of 0.90×10^6 and therefore are presented for only one Mach number. Increasing the Reynolds number to a value of 1.4×10^6 produced no noticeable effect on the $p_l/p_{t,2}$ distribution. The effect of increasing the angle of attack was to shift the stagnation point from the center of the flat face toward the windward side.

In figure 6 the surface Mach number on the cylinder is presented for a free-stream Mach number of 3.51 and a Reynolds number of 1.4×10^6 for the angle-of-attack range. With the model at an angle of attack of 0°, the corner effects extend to a z/D of approximately 0.45 and agree with the point-of-flow reattachment determined from shadowgraphs for the same free-stream conditions. Increasing the angle of attack resulted in a

decrease in the extent of the end effect on the windward side with the flow reattaching at a relatively short distance back of the leading edge. On the leeward side, however, for angles of attack over $7\frac{1}{2}^{\circ}$, the flow apparently remained separated over the entire cylinder length.

The local pressure distribution across the flat face of the cylinder expressed as u_l/a_t and computed from equation (1) is shown in figure 7 for a Mach number range from 2.49 to 4.44 and a Reynolds number range from 0.90×10^6 to 1.4×10^6. The spread which represents 20 to 40 data points is indicated by the vertical bars. There was no apparent trend of the data through the Mach number and Reynolds number ranges in this investigation. The curve is faired through the average u_l/a_t values for all stations except x/r equal 0.125. The very small pressure differentials from the stagnation point to this station, as indicated in figure 5 for an angle of attack of 0°, were within the accuracy of the recording equipment and produced slightly high values of u_l/a_t. It is assumed in fairing the curve of figure 7 that the u_l/a_t ratio varies linearly with x/r from the stagnation point, where u_l/a_t is zero, to an x/r of 0.25 where the pressure differential is greater than the accuracy of the recording equipment. The slope of this curve at $x/r = 0$ is the dimensionless velocity gradient parameter $\left(\dfrac{r}{a_t}\dfrac{du}{dx}\right)_{x=0}$ which governs the heat transfer to the stagnation point as discussed in reference 7. For the given Mach number and Reynolds number ranges this parameter was constant at approximately 0.3 and is in good agreement with the values obtained for a flat face in references 2 and 7.

Heat-Transfer Test

Flat face.- The measured heat-transfer coefficients at the stagnation point for an angle of attack of 0° for two Mach numbers and Reynolds numbers are presented in the following table:

M	R	h_t
2.49	0.77×10^6	0.00832
2.49	1.46	.01114
3.51	.75	.00762
3.51	1.31	.01022

Sibulkin's equation (ref. 3) for calculating the heat-transfer coefficient at the stagnation point of a hemisphere is as follows:

$$\frac{hD}{k} = 0.763 N_{Pr}^{0.4}\left(\frac{3u_\infty D\rho}{\mu}\right)^{1/2}$$

This equation can be expressed in terms of the free-stream conditions as

$$h\sqrt{D} = 0.67\sqrt{\frac{\beta D}{u_\infty}}\sqrt{\frac{u_\infty \rho_\infty}{\mu_\infty}}k_\infty\sqrt{\frac{T_t}{T_w}\frac{\rho_{t,2}}{\rho_\infty}\frac{\mu_\infty}{\mu_w}\left(\frac{k_w}{k_\infty}\right)^2}$$

where the Prandtl number is 0.72. The term $\beta D/u_\infty$ was considered to be invariant with Mach number by Sibulkin. The Sibulkin equation was modified to incorporate a variable $\beta D/u_\infty$ with Mach number that was determined by Korobkin (see ref. 8). Previous tests (ref. 2) have indicated the stagnation heat-transfer coefficient on a flat face is 55 percent of that for a hemisphere of the same diameter. The measured stagnation heat-transfer coefficients shown in figure 8 are in good agreement with 55 percent of the stagnation heat-transfer coefficient calculated from this equation for a hemisphere that includes the term $\beta D/u_\infty$ as a function of Mach number.

The influence of Mach number, Reynolds number, and angle of attack on the heat-transfer coefficient distribution over the flat face is also shown in figure 8. The local heat-transfer coefficient at each thermocouple location is expressed as a ratio to the stagnation heat-transfer coefficient at an angle of attack of 0°. At an angle of attack of 0°, the maximum value of the local heat-transfer coefficient was expressed as a ratio to the stagnation-point heat-transfer coefficient and is 1.2 for $M = 2.49$ and 1.3 for $M = 3.51$. The decrease in heat-transfer coefficient for x/r greater than 0.9 is believed to be due to conduction to the cylindrical portion of the body. Increasing the Reynolds number by a factor of almost two produced a negligible effect on $h_l/h_{t,2}$.

The effect of angle of attack is most noticeable in the region of high heating near the edge of the front face. On the windward edge the heat-transfer coefficients increase with increasing angle of attack. At a Mach number of 2.49, increasing the angle of attack from 0° to 15° increases the heat-transfer coefficient near the windward edge 34 percent for the higher Reynolds number as compared with 25 percent for the lower Reynolds number. At a Mach number of 3.51 and a Reynolds number of 1.3×10^6, increasing the angle of attack from 0° to 15° increases the local heat-transfer coefficient near the windward edge 20 percent. At

a Reynolds number of 0.75×10^6 the local heat-transfer coefficient increases 30 percent. However, it is to be noted that the increase of the local heat-transfer coefficients corresponding to a decrease in Reynolds number at a Mach number of 3.51 is apparently reversed at a Mach number of 2.49.

Cylinder wall.- The distribution of the heat-transfer coefficients on the cylindrical portion of the body is shown in figure 9. The extent of flow separation was determined from the shadowgraphs in figure 4 and the reattachment points are denoted by the solid symbols in figure 9. The results for M = 2.49 and R = 0.77×10^6 are shown in figures 9(a) and 9(b). The symmetry of h with z/D for the two rows of thermo-couples located diametrically opposite from each other is an indication of the repeatability of the data and the symmetry of the flow. At an angle of attack of 0° the region of low heat transfer in the low-density separated flow of the corner extends to z/D = 0.5. As a crude approxi-mation of the magnitude of the heat-transfer coefficient on the cylinder, the local heat transfer at z/D = 0.875 was calculated from the flat-plate theory in reference 9 by using the value of M determined from the static pressure and the measured total pressure and by assuming that the Reynolds number is based upon the distance from the point of flow reattachment (determined from the shadowgraphs). The calculated laminar heat-transfer coefficient was 68 percent low. When the same Mach number and flow length were used with the turbulent heat-transfer relations, the heat-transfer coefficient was only 16 percent low. The deviation can be due to errors in determining the absolute point of flow reattach-ment and corner effects; however, the Mach number distribution from pressure tests indicates the effects of the corner are negligible for z/D greater than 0.6. The heat-transfer coefficient is higher along the after portion of the cylinder at $\alpha = 0^\circ$ than on the windward edge for $\alpha = 7.5^\circ$ and 15°; this difference is considered to be an indication that the flow was turbulent at $\alpha = 0^\circ$. As the angle of attack is increased to 7.5°, the extent of flow separation decreases to z/D = 0.3 on the windward edge. At this angle of attack the resultant heat-transfer coefficient is approximately constant along the stagnation line and is in good agreement with the laminar heat-transfer coefficient for a swept cylinder of infinite length (ref. 10) denoted by the solid line. Increasing the angle of attack to 15°, the separation is confined to the immediate vicinity of the corner and is not discernible on the heat-transfer distribution. The measured h decreases with increasing dis-tance from the front face and is 15 percent greater than that predicted by swept-cylinder theory at the maximum z/D station.

On the leeward side (fig. 9(b)), no point-of-flow reattachment is visible for angles of attack of 7.5° and 15°. The region of low heat transfer is more extensive than on the windward face, but at an angle of attack of 7.5° near the base of the model the heat-transfer coefficient

is greater on the leeward side than on the windward side. Similar distributions were noted on a smooth cone (ref. 5) at an angle of attack with laminar heat transfer on the windward side and turbulent heat transfer on the leeward side. On the leeward side of the cylinder at an angle of attack of 15° the extensive flow separation caused very low heat-transfer coefficients.

The heat-transfer coefficients were determined only for the windward side at $M = 2.49$ and $R = 1.46 \times 10^6$ and are shown in figure 9(c). It should be noted that the ordinate scales are reduced by a factor of 2 in this figure due to the extremely high heat-transfer coefficients. The high heating on the rear portion of the cylinder at an angle of attack of 0° is an indication of a turbulent boundary layer. Similar high heating existed at angles of attack of 7.5° and 15°. The maximum values along the rear portion of the cylinder increase with angle of attack. The values from the laminar swept-cylinder theory for both angles of attack are much lower than those from the experimental data; this result further substantiates the fact that a turbulent boundary layer existed at both angles of attack.

The h distribution along the windward and leeward sides at $M = 3.51$ and $R = 0.75 \times 10^6$ is shown in figures 9(d) and 9(e) to be similar to the data for $M = 2.49$ with the exception that the flow is laminar along the entire cylinder at an angle of attack of 0°. The experimental data are in good agreement with calculated laminar heat-transfer coefficients using local Mach number and point-of-flow reattachment. The measured data at an angle of attack of 7.5° are in good agreement with swept-cylinder theory. At an angle of attack of 15° the experimental values near the front face are much greater than those predicted by the swept-cylinder theory but have reasonable agreement at the rearmost station. The h distribution on the leeward side (fig. 9(e)) shows no transition from laminar to turbulent.

The high Reynolds number data for $M = 3.51$ (fig. 9(f)) were obtained only on the windward side. At an angle of attack of 0°, the rearmost thermocouple indicates a turbulent boundary layer. At angles of attack of 7.5° and 15°, the heat-transfer distribution is very similar to that for the low Reynolds number data in figure 9(d), where experimental h values approach the laminar swept-cylinder theory at the rearmost thermocouple.

CONCLUDING REMARKS

Heat-transfer coefficients and pressure distributions were obtained on a 4-inch-diameter flat-face cylinder in the Langley Unitary Plan

wind tunnel. Stagnation-point heating to a flat-faced cylinder can be approximated by 55 percent of the value calculated by using a modification of Sibulkin's theory for a hemisphere with an acceptable degree of accuracy for Mach numbers from 2.49 to 3.51. The dimensionless velocity gradient parameter $\left(\dfrac{r}{a_t}\dfrac{du}{dx}\right)_{x=0}$ for an angle of attack of $0°$ at the stagnation point was constant for a Mach number range from 2.49 to 4.44 and a Reynolds number range from 0.9×10^6 to 1.4×10^6.

The heat transfer to the cylindrical afterbody at an angle of attack of $0°$ for both laminar and turbulent boundary layer can be approximated by flat-plate theory with the origin of the boundary layer being located at the point-of-flow reattachment downstream of the flat face. With the model at an angle of attack, swept-cylinder theory gave acceptable approximations of the heating along the cylinder stagnation line. This theory is based on a cylinder of infinite length; therefore, in the vicinity of the cylinder leading edge the agreement is relatively poor, but for large distances from the front face the theory was applicable for a laminar boundary layer.

Langley Research Center,
    National Aeronautics and Space Administration,
        Langley Field, Va., March 12, 1959.

REFERENCES

1. Eggers, Alfred J., Jr., Allen, H. Julian, and Neice, Stanford E.: A
   Comparative Analysis of the Performance of Long-Range Hypervelocity
   Vehicles. NACA TN 4046, 1957. (Supersedes NACA RM A54L10.)

2. Stoney, William E., Jr., and Swanson, Andrew G.: Heat Transfer
   Measured on a Flat-Face Cylinder in Free Flight at Mach Numbers up
   to 13.9. NACA RM L57E13, 1957.

3. Sibulkin, M.: Heat Transfer Near the Forward Stagnation Point of a
   Body of Revolution. Jour. Aero. Sci. (Readers' Forum), vol. 19,
   no. 8, Aug. 1952, pp. 570-571.

4. Anon.: Manual for Users of the Unitary Plan Wind Tunnel Facilities
   of the National Advisory Committee for Aeronautics. NACA, 1956.

5. Burbank, Paige B., and Hodge, B. Leon: Distribution of Heat Transfer
   on a 10° Cone at Angles of Attack from 0° to 15° for Mach Numbers
   of 2.49 and 4.65 and a Solution to the Heat-Transfer Equation That
   Permits Complete Machine Calculations. NASA MEMO 6-4-59L, 1959.

6. Ames Research Staff: Equations, Tables, and Charts for Compressible
   Flow. NACA Rep. 1135, 1953. (Supersedes NACA TN 1428.)

7. Stoney, William E., Jr., and Markley, J. Thomas: Heat Transfer and
   Pressure Measurements on Flat-Faced Cylinders at Mach Number 2.
   NACA TN 4300, 1958.

8. Korobkin, Irving: Laminar Heat Transfer Characteristics of a Hemis-
   phere for the Mach Number Range 1.9 to 4.9. NAVORD Rep. 3841,
   (Aeroballistic Res. Rep. 257), U. S. Naval Ord. Lab. (White Oak,
   Md.), Oct. 10, 1954.

9. Van Driest, E. R.: The Problem of Aerodynamic Heating. Aero. Eng.
   Rev., vol. 15, no. 10, Oct. 1956, pp. 26-41.

10. Goodwin, Glen, Creager, Marcus O., and Winkler, Ernest L.: Investiga-
    tion of Local Heat-Transfer and Pressure Drag Characteristics of a
    Yawed Circular Cylinder at Supersonic Speeds. NACA RM A55H31, 1956.
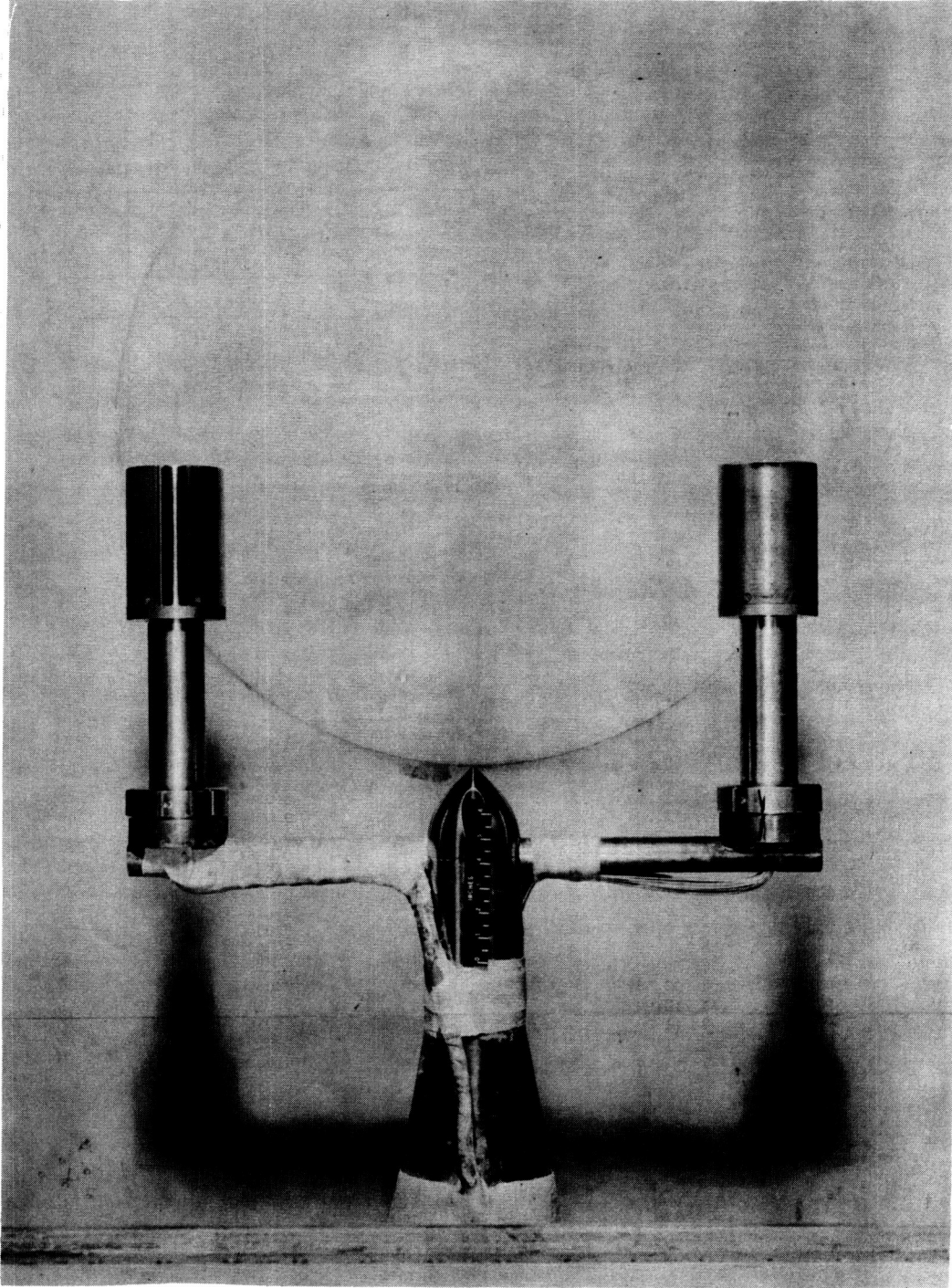
Figure 1.- Heat-transfer and pressure models mounted for test.   L-57-4218
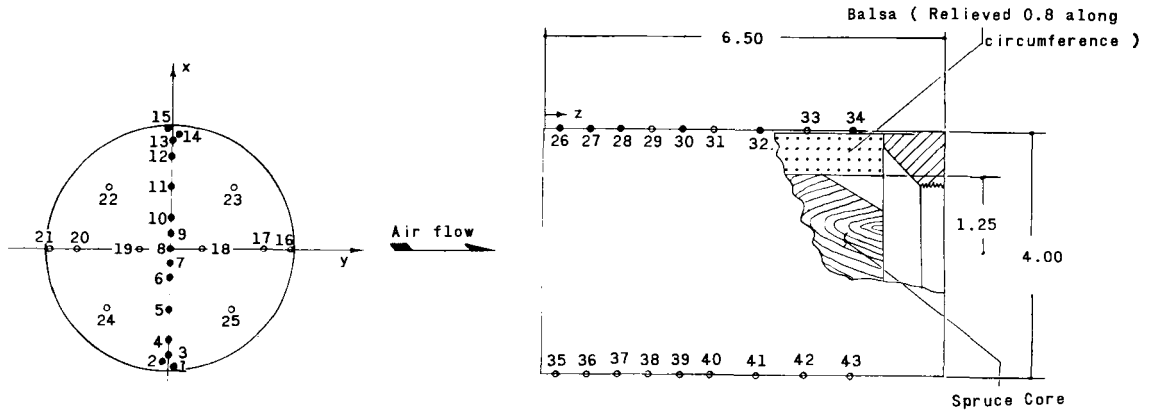
Thermocouple and orifice No.	Thickness	Location y	x
1	0.033	0.10	-1.95
2	0.033	-0.10	-1.85
3	0.033	0.00	-1.75
4	0.032	0.00	-1.50
5	0.032	0.00	-1.00
6	0.032	0.00	-0.50
7	0.032	0.00	-0.25
8	0.033	0.00	0.00
9	0.033	0.00	0.25
10	0.032	0.00	0.50
11	0.033	0.00	1.00
12	0.032	0.00	1.50
13	0.033	0.00	1.75
14	0.033	0.10	1.85
15	0.033	-0.10	1.95
16	0.033	1.95	0.00
17	0.033	1.50	0.00
18	0.032	0.50	0.00
19	0.032	-0.50	0.00
20	0.032	-1.50	0.00
21	0.033	-1.95	0.00
22	0.033	-1.00	1.00
23	0.031	1.00	1.00
24	0.032	-1.00	-1.00
25	0.032	1.00	-1.00

$\bullet, \circ$ $M = 2.49;$ $R = 0.77 \times 10^6$

$\bullet$ $M = 2.49;$ $R = 1.46 \times 10^6$

$\bullet$ $M = 3.51;$ $R = 1.31 \times 10^6$

Thermocouple and orifice No.	Thickness	Location z
26	0.033	0.25
27	0.028	0.75
28	0.030	1.25
29	0.030	1.75
30	0.029	2.25
31	0.029	2.75
32	0.031	3.50
33	0.031	4.25
34	0.031	5.00
35	0.033	0.25
36	0.028	0.75
37	0.029	1.25
38	0.030	1.75
39	0.030	2.25
40	0.030	2.75
41	0.030	3.50
42	0.030	4.25
43	0.031	5.00

Figure 2.- Details of model and thermocouple location. All dimensions are in inches.
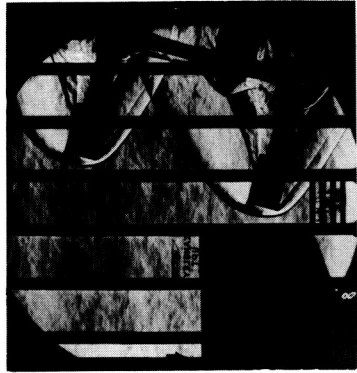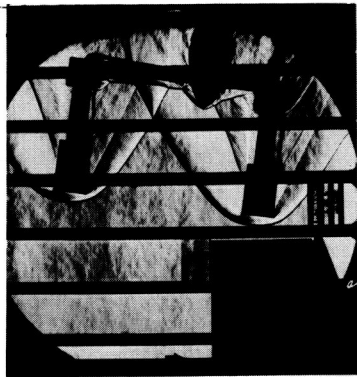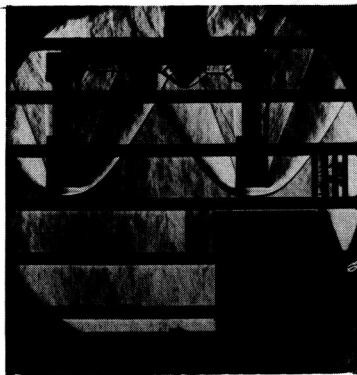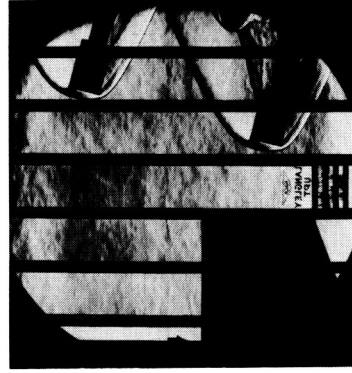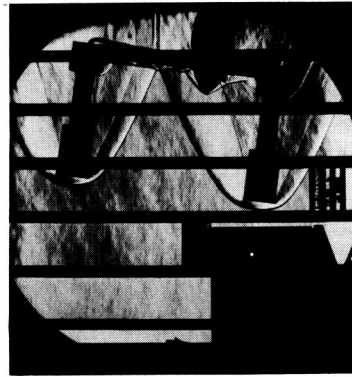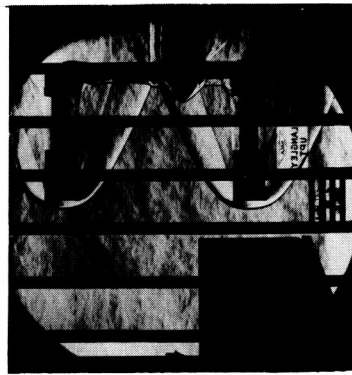
(a) M = 2.49; R = 0.90 × 10⁶.

(b) M = 3.51; R = 0.90 × 10⁶.

L-59-1892

Figure 3.- Typical schlieren photographs of heat-transfer and pressure models.

$\alpha = 7.5°$

L-59-1893

$\alpha = 0°$
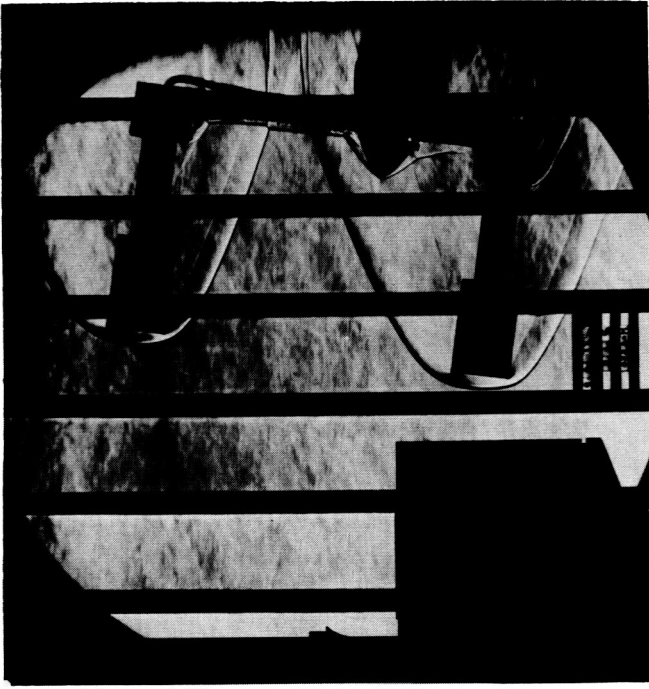
(c) M = 4.44; R = 0.90 × 10⁶.

Figure 3.- Concluded.

α = 15.0°

α = 7.5°

α = 0°

(a) M = 2.49; R = 0.90 × 10⁶.

α = 15.0°

α = 7.5°

α = 0°
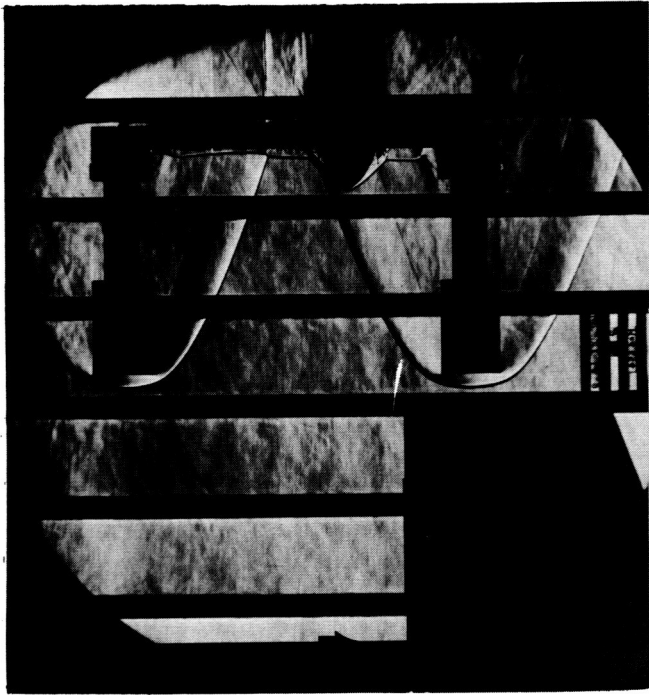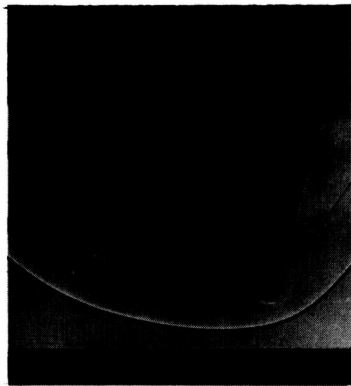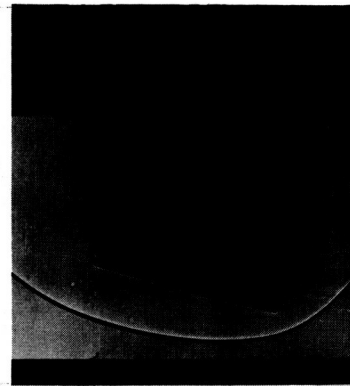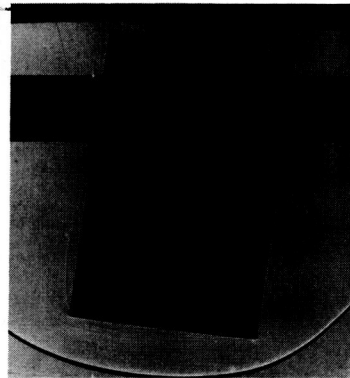
(b) M = 3.51; R = 0.90 × 10⁶.

L-59-1894

Figure 4.- Typical shadowgraph photographs of a right circular cylinder.

α = 0°

α = 7.5°
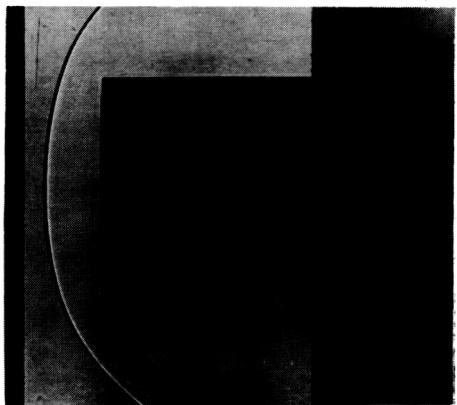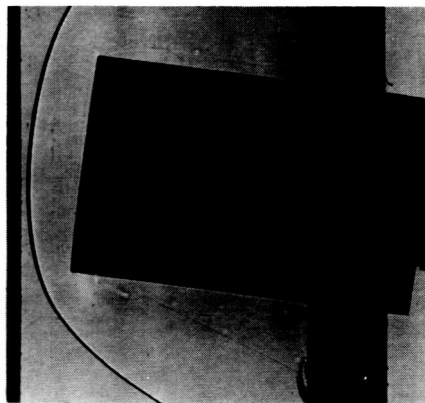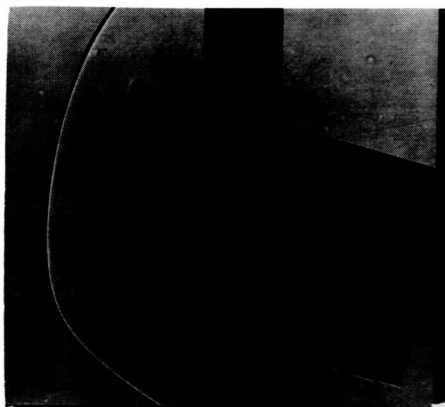
α = 15.0°

(c) M = 4.44; R = 0.90 × 10^6.

L-59-1895

Figure 4.- Concluded.
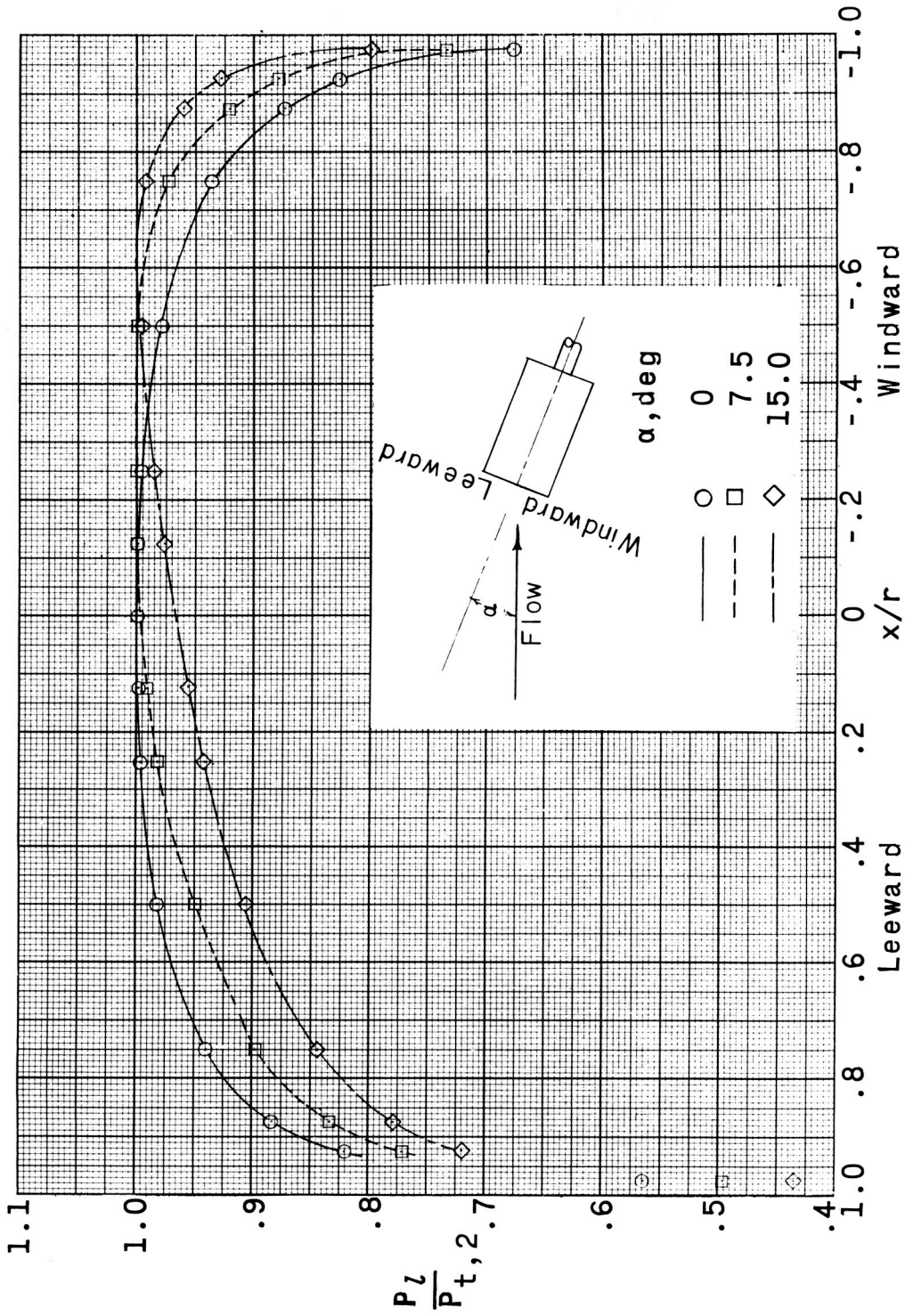
Figure 5.- Effect of angle of attack on the ratio of local pressures across the front face to the local pressure at the stagnation point for an angle of attack of 0°. M = 2.49; R = 0.90 × 10^6.
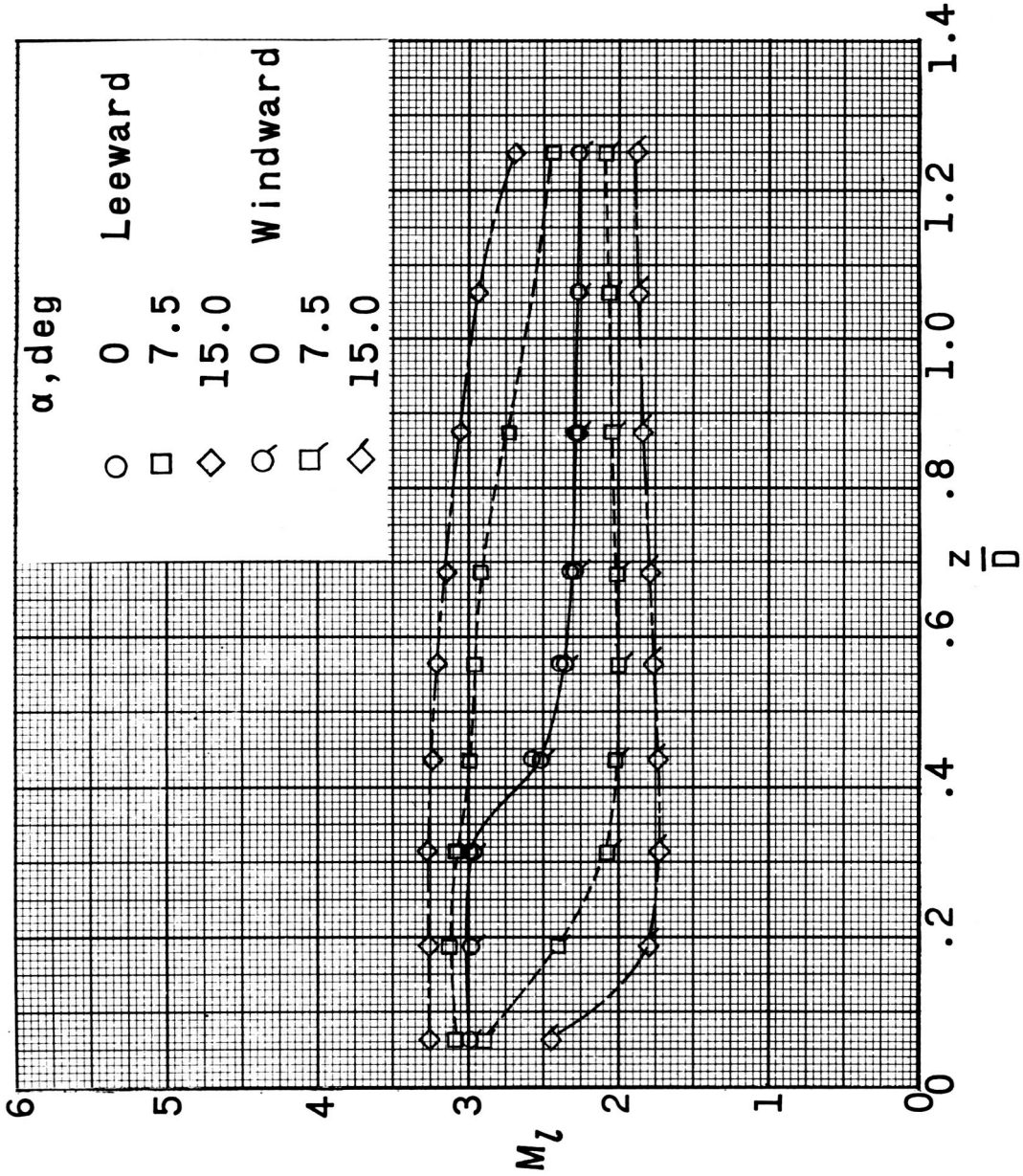
Figure 6.- Mach number distribution along cylindrical afterbody. M = 3.51; R = 1.4 × 10⁶.
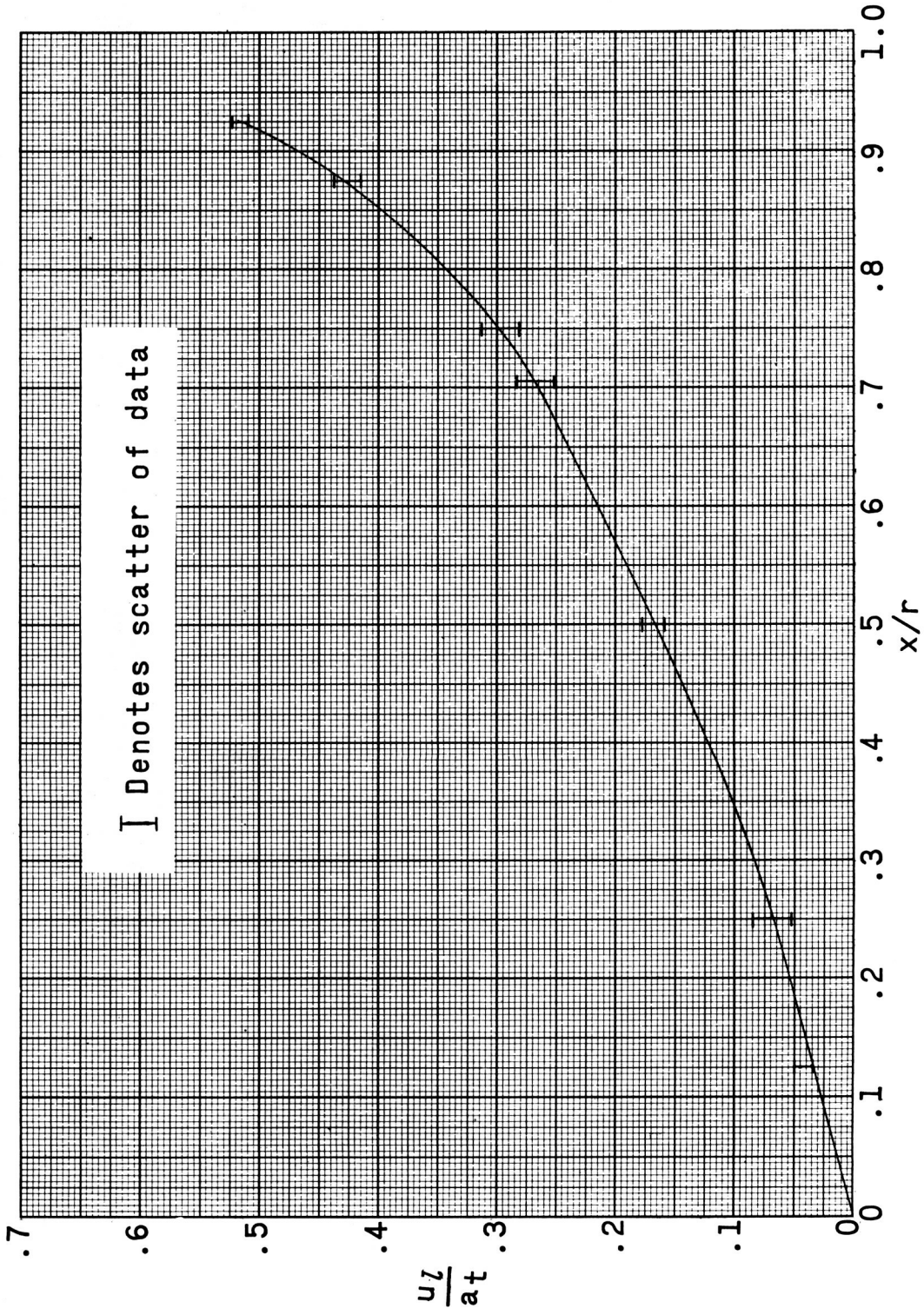
Figure 7.- The ratio of u_l/a_t across the flat face for a Mach number range of 2.49 to 4.44 and Reynolds number range 0.9×10^6 to 1.4×10^6. $\alpha = 0^{\circ}$.

22
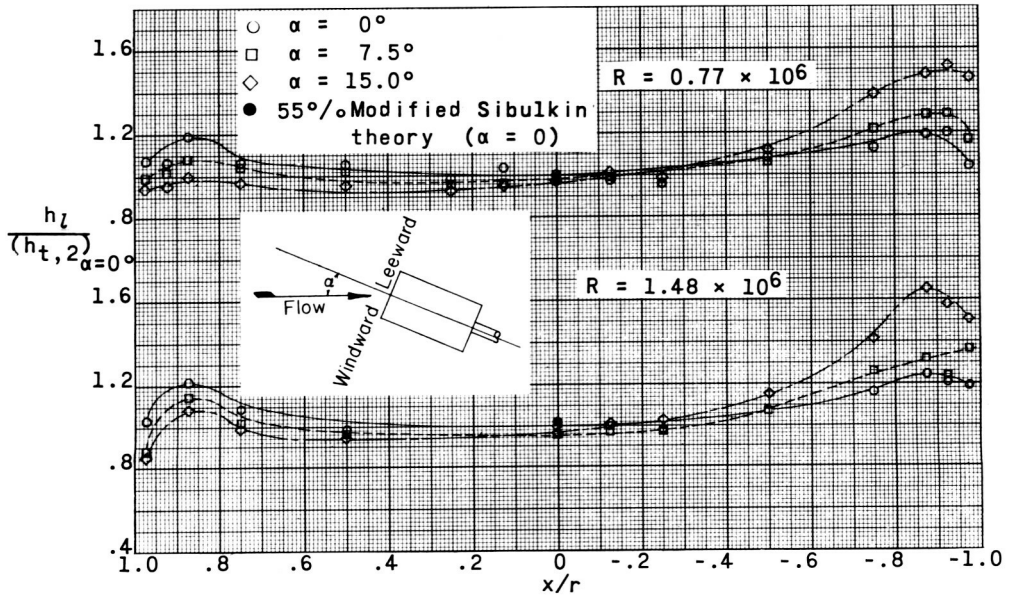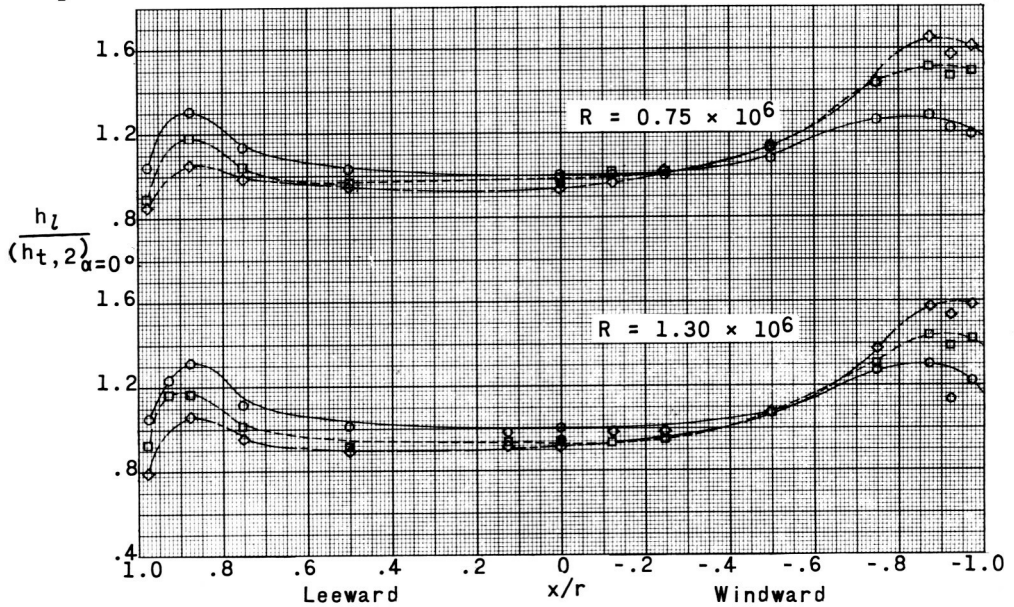
(a) M = 2.49.

(b) M = 3.51.

Figure 8.- Effects of Mach number, Reynolds number, and angle of attack on the heat-transfer distribution across the flat face.
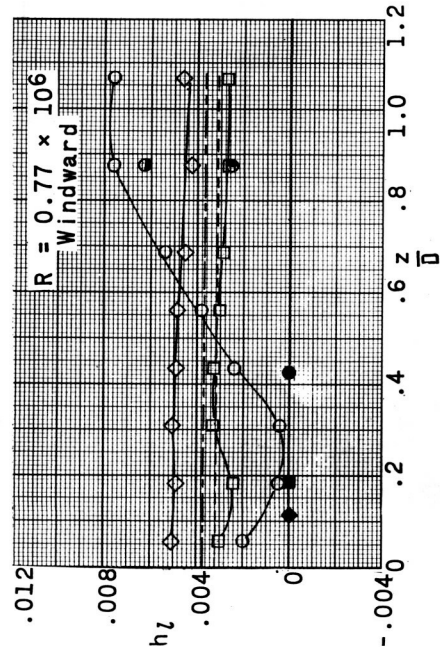
(a) M = 2.49
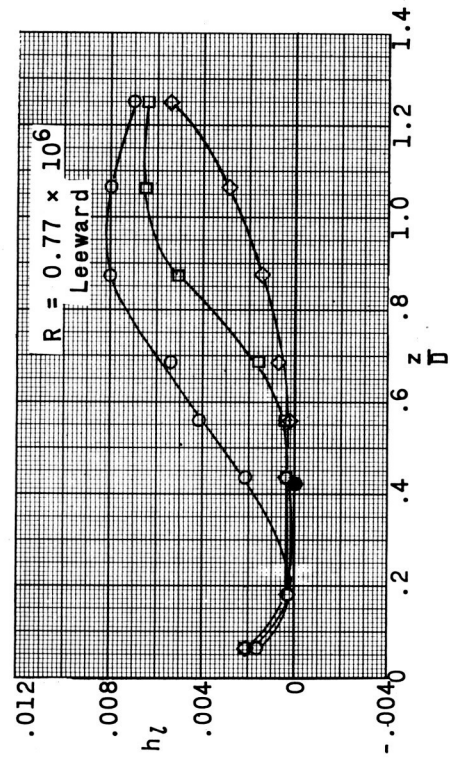
(b) M = 2.49.
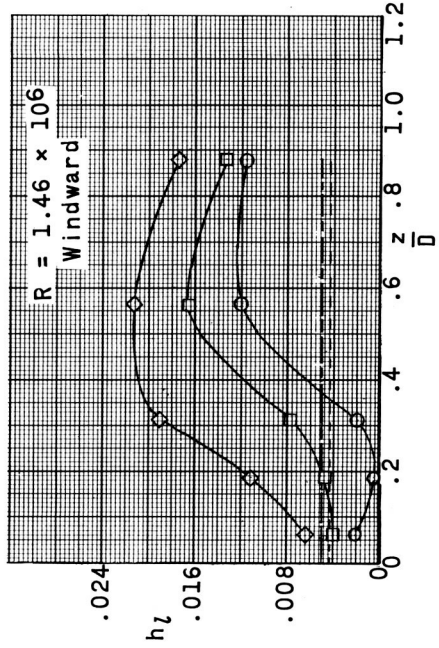
(c) M = 2.49.
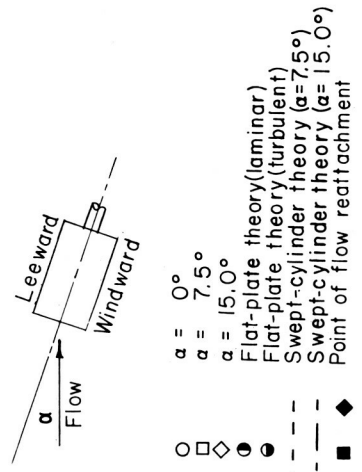
Figure 9.- Effect of Mach number, Reynolds number, and angle of attack to the heat transfer distribution along the cylindrical afterbody.
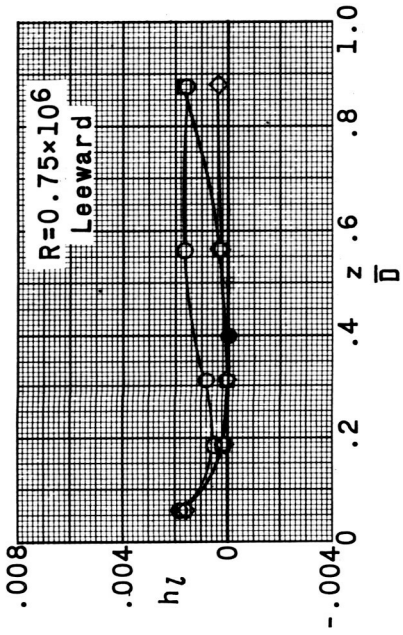
(e) M = 3.51.
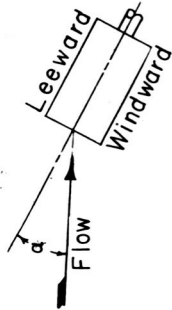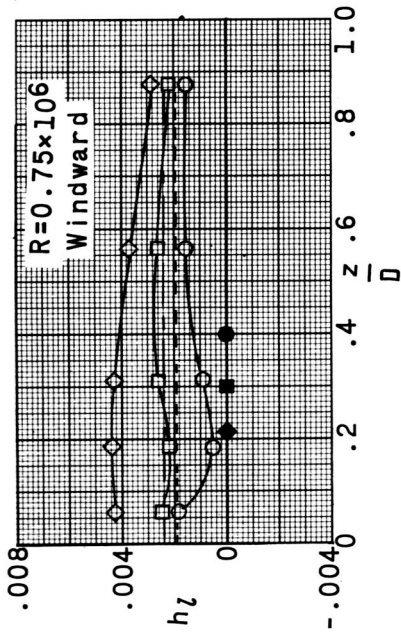
(d) M = 3.51.
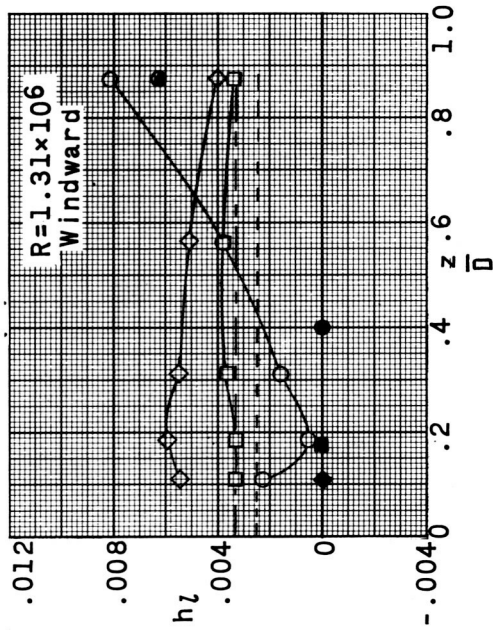
(f) M = 3.51.

Figure 9.- Concluded.